Comparisons of the dynamical characteristics of a semi-submersible floating offshore wind turbine based on two different blade concepts

Jiahao Chen [a,c], Zhiqiang Hu [b,*], Decheng Wan [a,c], Qing Xiao [d]

[a] State Key Laboratory of Ocean Engineering, Shanghai Jiao Tong University, Shanghai 200240, China
[b] School of Engineering, Newcastle University, Newcastle upon Tyne, NE1 7RU, UK
[c] Collaborative Innovation Center for Advanced Ship and Deep-Sea Exploration, Shanghai Jiao Tong University, Shanghai, China
[d] Department of Naval Architecture, Ocean and Marine Engineering, University of Strathclyde, Glasgow G4 0LZ, UK

ABSTRACT

Scaled model tests are important for the development and validation of floating offshore wind turbines. However, it has been found that Reynolds number dissimilitude between scales deteriorates the aerodynamic performance of floating offshore wind turbines when using model test investigation methodologies. To overcome this challenge, a semi-submersible floating offshore wind turbine model test with two different solutions, namely a geometrically matched blade model and a performance-matched blade model, was conducted in a wind/wave basin. Subsequently, a series of comparisons of the dynamical characteristics of these two models were made to clarify the respective validity of the two models and provide references for future floating offshore wind turbine model optimization. It is found that both model methods are capable of reflecting the essential dynamical characteristics but there are some differences in system eigenfrequencies and response amplitudes. Compared with the geometrically matched blade model, the performance-matched blade model has enhanced aerodynamic performance. Nevertheless, the overweight blades within the performance-matched blade model yields inevitable discrepancies compared with the original design.

1. Introduction

As climate change issues worsen with environmental pollution as a result of fossil energy usage, the development of offshore wind turbines has quickened in recent decades. Generally, offshore wind turbines are divided into two categories (Jeon et al., 2013), namely, bottom-mounted offshore wind turbines and floating offshore wind turbines (hereafter, FOWTs). Compared with the bottom-mounted turbines, which are usually limited to water depths of 30 m, FOWTs are capable of taking advantage of stronger and steadier wind resources in deeper water regions for more economical applications (Muliawan et al., 2013; Ma et al., 2015).

The dynamical properties of FOWTs are nonlinear and multidisciplinary (Coulling et al., 2013), including aerodynamics, hydrodynamics, structural dynamics, control algorithms and power electronics. Currently, model tests in wind/wave basins are still an irreplaceable study method for FOWTs. Compared with onsite measurements for full-scale demonstrations, scaled model tests have fewer risks, require less time and resources, and demonstrate better controls and repeatable

environmental conditions. Compared with numerical simulations, results from model tests are usually more feasible, and even numerical tools occasionally are verified using experimental results (Dunbar et al., 2015).

To date, a series of FOWT model tests have been conducted worldwide (Duan et al., 2016a; Koo et al., 2014; Wan et al., 2015). Unfortunately, unlike conventional offshore structure experiments that only apply Froude scaling scheme, Reynolds scaling is also a significant requirement for FOWT model tests, because aerodynamic loads are highly dependent on the Reynolds number. However, it is well known that the simultaneous maintenance of both Froude and Reynolds scaling in basin tests is impossible. Nevertheless, when applying only Froude scaling, the Reynolds number will decrease from full scale to model scale, insomuch that the thrust force, the rotor torque and the power of the FOWT model will be substantially lower than the desired (Martin, 2011). Additional details regarding this phenomenon will be discussed in sections 2.1 and 2.2.

Currently, there are a small number of solutions for the Reynolds number dissimilitude problem in FOWT model tests. These solutions can be roughly categorized into four types, namely, the 'wind discs model

---

Table 1
Froude scaling of the experimental parameters.

Parameters	Unite	Scaling factor
Length	m	λ
Time	s	$\lambda^{0.5}$
Frequency	1/s or rad/s	$\lambda^{-0.5}$
Mass	kg	λ^3
Force	N	λ^3
Moment	N.m	λ^4
Acceleration	m/s^2	1
Velocity	m/s	$\lambda^{0.5}$
Angle	$^\circ$	1

Fig. 2. Comparison of (a) performance-matched blades and (b) geometrically matched blades.

method', 'adjustable wind speed method', 'roughened blade leading edge method' and 'redesigned performance-matched blade method', which are discussed below:

(1) Wind discs model method (Wan et al., 2014): a turbine rotor is modelled as a stationary disc, and different size discs are utilized to emulate different aerodynamic loads on the rotor in different conditions. For example, a small disc is used in low-wind-speed operating conditions or the rotor-park conditions, but a large disc is used in high-wind-speed operating conditions. In spite of the thrust force being properly emulated, other aerodynamic properties, such as aerodynamic torque, gyroscopic effects, aerodynamic damping effects, etc., are generally emulated improperly.

(2) Adjustable wind speed method (Martin et al., 2014): a straightforward method to adjust wind speed to match the desired thrust force in model tests. However, the changes of model wind speed could exert an undesirable excess drag on irrotational structures (e.g. the tower or nacelle). Moreover, aerodynamic torque is still improper between scales.

(3) Roughened blades leading edge method (Martin, 2011): the leading edges of the blades are roughened, and the boundary layer (which is attached to the airfoil surface) is switched from laminar to turbulent flow to improve the lift and drag coefficient in low-Reynolds number model conditions. However, this method has a marginal effect on the improvement of the aerodynamic performance and yields some erratic performances in blade aerodynamic loads concomitantly.

(4) Redesigned performance-matched blades method (Martin et al., 2014): in 2011, the DeepCwind Consortium and the University of Maine carried out a series of FOWT model tests at the MARIN (Marine Research Institute Netherland) offshore basin for the OC4 project (Robertson et al., 2013). During the tests, Martin et al. (2014) found that the aerodynamic performance of geometrically

similar blades was dissatisfactory using the 'adjustable wind speed method' or 'roughened blade leading edge method' in low-Reynolds number model environments. Afterwards, they proposed the 'performance-matched blades' concept to improve aerodynamic performances for scaled FOWT model tests. In this method, the shape of the blade section is redesigned to match the desired aerodynamic performance in low-Reynolds number model environments. This concept was implemented in 2013, and some of the anterior FOWT model tests have been re-conducted at the MARIN (Goupee et al., 2014). In the same year, geometrically similar blades and redesigned performance-matched blades were also applied to a spar-type and semi-submersible FOWT model test at the SJTU (Shanghai Jiao Tong University) Deepwater Offshore Basin (Duan et al., 2016b)

Although the observed aerodynamic performance was improved using the performance-matched model blades, the model blades were inevitably overweight relative to the design specifications both in MARIN and SJTU model tests (Duan et al., 2016b; Goupee et al., 2014; Gueydon, 2016), which may induce a change in the dynamical characteristics of the FOWT models. Both the 'adjustable wind speed method' with geometrically matched (geometrically similar) blades and the 'redesigned performance-matched blades method' have their own known respective disadvantages. The 'adjustable wind speed method' with geometrically matched blades was applied to most of the previous FOWT model tests, and the 'redesigned performance-matched blades method' is a relatively new concept. Hence, the dynamical characteristics of the FOWT models
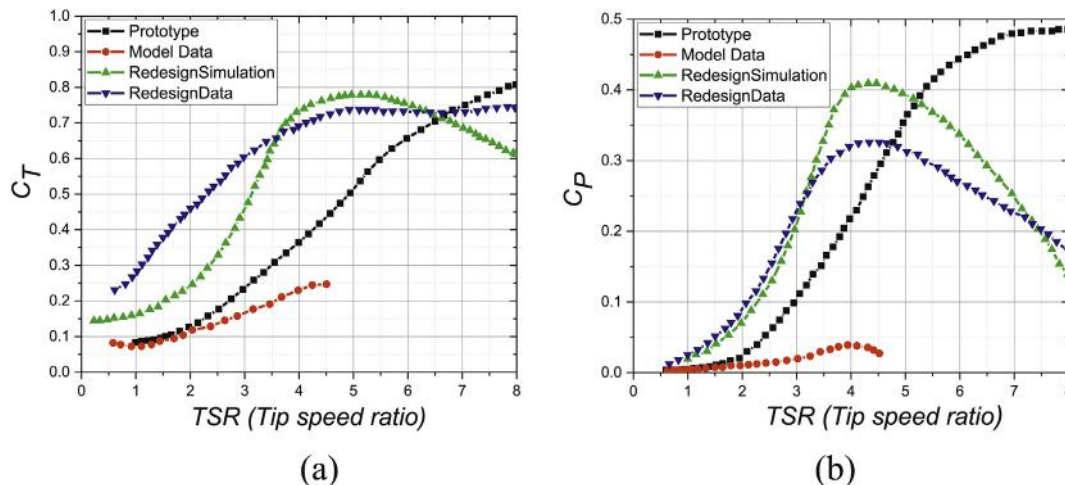

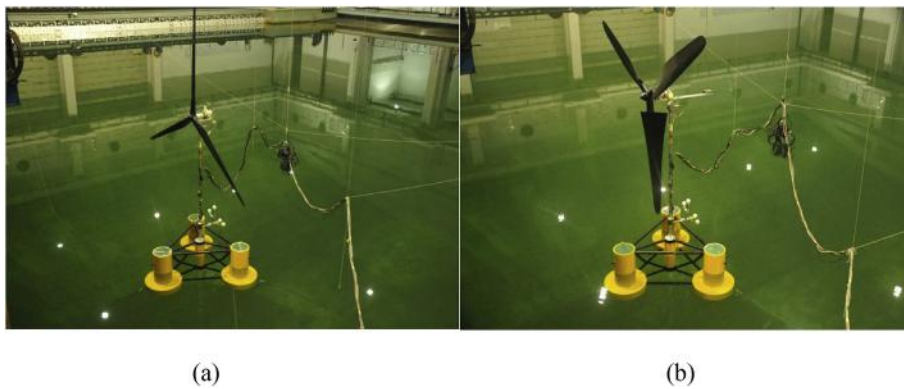**Fig. 1.** Comparison of the aerodynamic coefficients (Fowler et al., 2013).

Fig. 3. Comparison of (a) geometrically matched blade model and (b) performance-matched blade model.

Table 2
Mass properties of wind turbines components at full scale.

Item	Design		GMBS		PMBS	
	Mass(kg)	CM(m)	Mass(kg)	CM(m)	Mass(kg)	CM(m)
Blades (3)	53,220	90.00	52,659	90.65	319,800	90.65
Hub	56,780	90.17	57,272	90.65	57,272	90.65
Nacelle	240,000	89.35	232,291	90.65	470,347	90.65
Tower	249,718	43.40	287,128	51.00	287,128	51.00
Cables&Sensors	0	0	120,182	53.16	120,181	53.20
Total wind turbine	599,718	70.35	749,532	69.45	1,254,728	77.99

Table 3
Mass properties of the platforms at full scale.

Item	Design	GMBS	PMBS
Platform Mass with ballast (kg)	13,144,375	12,878,750	12,397,125
Platform centre of mass (m)	−13.46	−13.5	−13.5
Platform Roll Inertia (Kg.m2)	6,659,375,000	6,310,000,000	6,135,312,500
Platform Pitch Inertia (Kg.m2)	6,659,375,000	6,310,000,000	6,135,312,500
Platform Yaw Inertia (Kg.m2)	11,960,937,500	Not measured	Not measured

Table 4
Mass properties of the system at full scale.

Item	Design	GMBS	PMBS
System total mass (kg)	13,744,093	13,628,282	13,651,853
System centre of mass (m)	−9.80	−8.94	−5.09

based on these two different blade concepts are in urgent need of detailed comparison to further clarify their respective validity. In addition, comparing these two model methods will help to understand the sensitivity of a FOWT to aerodynamical characteristics and the mass distribution and will be beneficial to the optimization of the FOWT design and relevant model test technologies in the future.

Accordingly, Duan et al. (2016b) compared the dynamical characteristics of an OC3 spar-type FOWT with these two different blade methods and discovered interesting dynamical differences between the two methods. In Duan's research, however, the influences exerted by the blade masses were not sufficiently analysed, despite the existence of some essential differences between spar-type and semi-submersible FOWTs. Goupee et al. (2014) demonstrated the aerodynamic performance superiority of the performance-matched blades but also revealed particular impacts resulting from using overweight blades. Therefore, more detailed and comprehensive investigations of these different blades concepts would be significant.

This paper compares and analyses the dynamical properties of an OC4 semi-submersible FOWT with two different blade concepts in detail, including the investigation of 6-DOF motion, aerodynamic damping effects, gyroscopic effects, tower-top structure dynamic responses and

mooring system dynamical impacts. Meanwhile, this paper also presents solutions for the Reynolds number dissimilitude and mass distribution problems, in addition to the corresponding experimental details. In general, the content in this paper utilized as a reference to contribute guidance to researchers who also want to conduct similar or improved FOWT model tests.

2. Material and methods

2.1. Scaling methodology

In most cases, the FOWT system is subjected to wind and wave loads simultaneously. In other word, Froude number scaling (usually used for wave loads scaled in offshore structures model tests) and Reynolds number scaling (usually used for wind loads scaled in wind turbines model tests) actually should be satisfied simultaneously in the FOWT model tests. However, Reynolds number scaling is impractical in a typical wind/wave basin environment. Therefore, Froude number scaling instead of Reynolds number scaling was applied to the FOWT model tests, actually. Froude number Fr is defined as the ratio of inertia forces to gravity forces:

$$Fr = \frac{V}{\sqrt{gL}} \tag{1}$$

where V is the fluid velocity, L is the characteristic length, g is the acceleration of gravity.
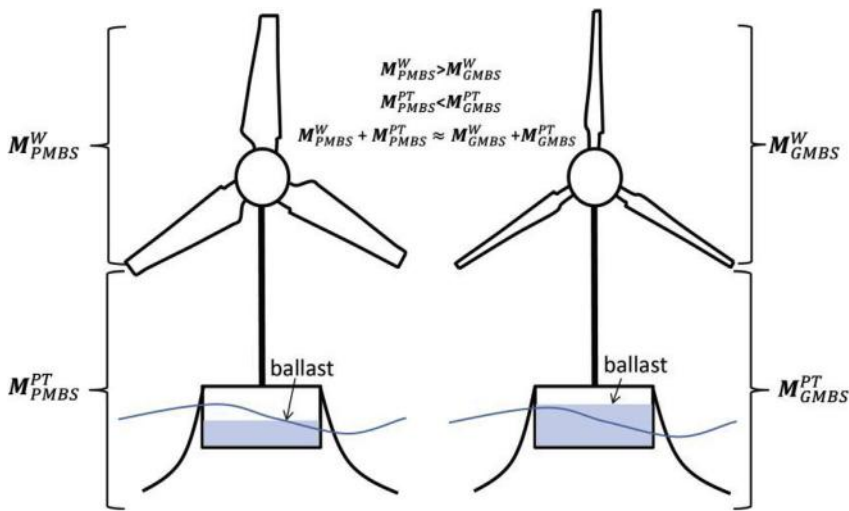
In the test, a geometric scaling factor λ is:

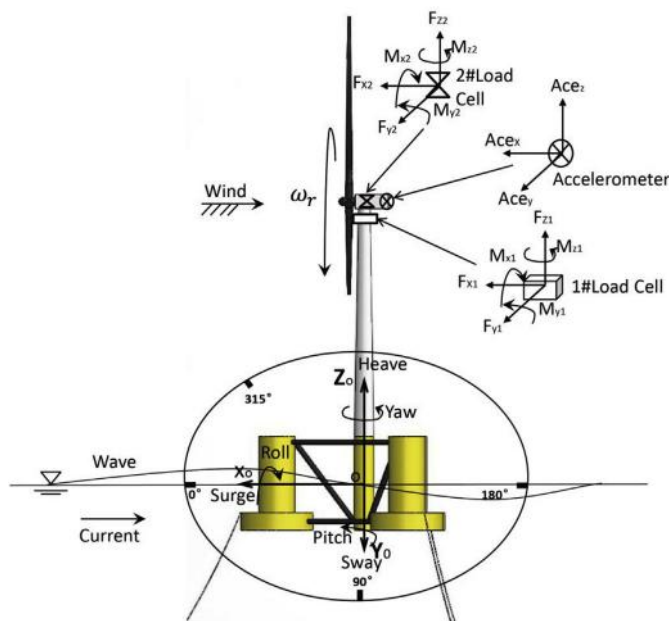**Fig. 4.** Schematic diagram of mass distribution between models.

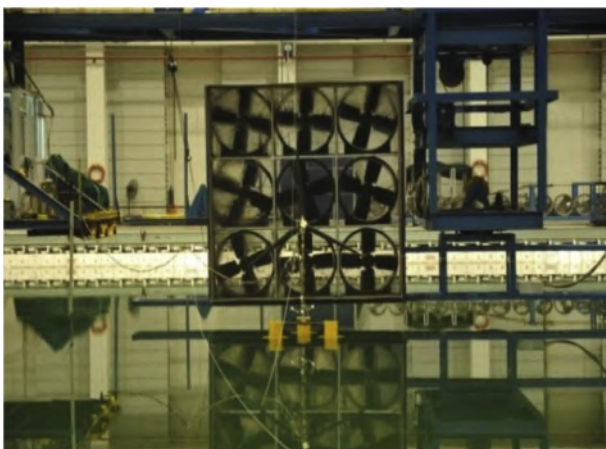**Fig. 5.** Reference coordinates and sensors of the experimental model.

Fig. 6. Overview of the wind generation system.

$$\lambda = \frac{L_f}{L_m} = 50:1 \tag{2}$$

where the subscript 'f' denotes the full scale, and the subscript 'm' denotes the model scale.

In addition, the Froude number between scales should be equivalent according to the Froude number scaling laws, yielding:

$$Fr_f = Fr_m \tag{3}$$

Substituting Eq. (1) into Eq. (3), yielding:

$$V_f/V_m = \sqrt{L_f/L_m} = \lambda^{0.5} \tag{4}$$

According to the geometric scaling factor and the Froude number scaling laws mentioned above, more parameters scaling are derived by a dimensional analysis method, shown in Table 1.

Reynolds number, which is the ratio of inertia forces to viscous forces for fluid flow, defined as:

$$Re = \frac{\rho V L}{\mu} \tag{5}$$

where ρ is the fluid density, V is the fluid inflow velocity, L is a characteristic length, μ is the dynamic viscosity coefficient.

According to Table 1, Reynolds number between scales is given by:

$$\frac{Re_f}{Re_m} = \frac{\rho V_f L_f/\mu}{\rho V_m L_m/\mu} = \frac{V_f}{V_m} \times \frac{L_f}{L_m} = \lambda^{1.5} \tag{6}$$

As can be seen in Eq. (6), according to the Froude number scaling laws, Reynolds number at full scale is much larger than that at model scale. Preliminary verifications were done by Fowler et al. (2013) and Martin (2011). It was found that the flow condition transformed from turbulent flow (full scale) to laminar flow (model scale) with Reynolds number decreasing from full scale to model scale. All these changes finally results in large differences in aerodynamic performances between scales.

Table 5
Aerodynamic information between models in three wind cases.

Desired					
	Rotor Thrust	kN	276.0	770.4	451.1
	Wind speed	m/s	5.0	11.4	18.0
GMBS	1P	rad/s	0.83	1.51	1.14
	3P	rad/s	2.48	4.52	3.42
PMBS	1P	rad/s	1.05	1.02	1.29
	3P	rad/s	3.14	3.05	3.86

Fig. 7. Tower construction (Duan et al., 2016a).

Table 6
Natural frequencies and damping ratios for 6-DOF motion between the two models.

Motion Mode	Frequency (rad/s)		Damping Ratio	
	GMBS	PMBS	GMBS	PMBS
Surge	0.12	0.10	0.06	0.09
Sway	0.11	0.09	0.05	0.08
Heave	0.38	0.38	0.02	0.01
Roll	0.26	0.16	0.03	0.04
Pitch	0.26	0.17	0.05	0.05
Yaw	0.14	0.13	0.03	0.03

since the actual wind speed is significantly adjusted to match the desired rotor thrust force, other characteristics, such as the tip speed ratio, rotor torque moment, aerodynamic damping, etc., may differ across scales. Moreover, when subjected to wind and wave loads in basin tests, the aerodynamic performance of geometrically matched blades will be affected by large amplitude motions from the floating platform and are thus likely to be unstable. Regarding the 'redesigned performance-matched blades method', some preliminary investigations (Fowler et al., 2013; Goupee et al., 2014) have been conducted to prove that it constitutes a more effective way to improve the aerodynamic performance for FOWT model tests. As observed in Fig. 1 (wherein 'Prototype' denotes the design value; 'Model Data' denotes the measured results in the model test after applying geometrically matched blades; 'Redesign Simulation' denotes the numerical simulation results using performance-matched blades; and 'Redesign Data' denotes the measured results in the model test after applying performance-matched blades), the thrust force coefficient C_T and the power coefficient C_P of the redesigned performance-matched blades (a modified Drela AG24 airfoil was used here; refer to (Fowler et al., 2013) for more details) are closer to the prototype in low-Reynolds number model conditions generally.

The modified Drela AG24 airfoil mentioned above was also used to redesign the performance-matched blades in our experiments. The geometrically matched blades and redesigned performance-matched blades are compared in Fig. 2, from which it is apparent that the chord length of the performance-matched blade (see Fig. 2a) is much larger than that of the geometrically matched blade (see Fig. 2b). Thus, the performance-matched blade is not as susceptible to laminar separation as the geometrically matched blades in low-Reynolds-number model conditions, which improves its aerodynamic performance (Martin, 2011). More details about the design of these two types of blades can be found in the supporting literature (Duan et al., 2016b; Fowler et al., 2013).

In the remainder of the sections herein, the FOWT with geometrically matched blades is referred to as a 'geometrically matched blades system' (GMBS), whereas that with redesigned performance-matched blades is referred to as a 'performance-matched blades system' (PMBS).

2.3. Model description and calibration tests

2.3.1. Model description

With the ambition of investigating the different dynamical characteristics of FOWTs due to the effects of GMBS and PMBS blades, a model test was conducted in the SJTU (Shanghai Jiao Tong University) Deepwater Offshore Basin (see Fig. 3). An OC4 DeepCwind semi-submersible floating platform (Robertson et al., 2012) was selected as the floating supporter, and an NREL 5-MW reference wind turbine (Jonkman et al., 2009) was mounted on this platform. More details about the OC4 DeepCwind semi-submersible FOWT can be found in (Robertson et al., 2012).

Mass distribution of the FOWT is one of the key points that must be considered carefully in the model tests. According to the Froude scaling laws, the target length of the model blade is 1.23 m (61.5 m at full scale), and the mass is only 138 g at the model scale. A hollow structure fabricated by a woven-carbon-fibre-epoxy composite material was used to
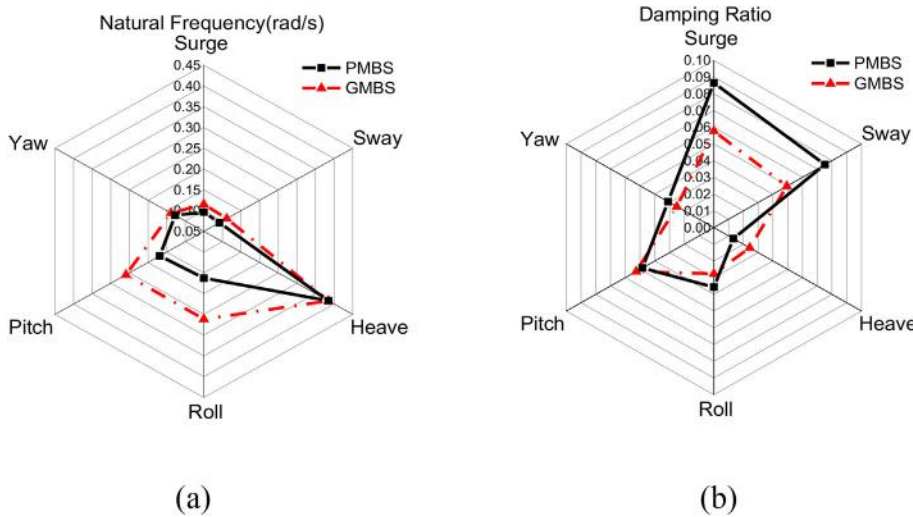

Fig. 8. Tower eigenfrequencies.

2.2. Solutions to address Reynolds number dissimilitude

Regarding the aforementioned Reynolds number dissimilitude problem, this paper utilizes two solutions, namely the 'adjustable wind speed method' with geometrically matched blades and the 'redesigned performance-matched blades method', respectively. In the 'adjustable wind speed method', the wind turbine with geometrically matched blades is fixed 3 m downstream from the wind generator system. Then, the power of the wind generator system is adjusted until the aerodynamic thrust force is equivalent to the desired value. Nevertheless,

Fig. 9. Comparisons of (a) natural frequencies and (b) damping ratio.

Table 7
Test matrix.

Case type	Load case	Wind speed(m/s)	Wave		
			H_s(m)	T_p(s)	ɣ
Wind only	LC1	5	0	0	0
	LC2	8	0	0	0
	LC3	11.4	0	0	0
	LC4	18	0	0	0
Combined wind and wave	LC5	0	0	3.5–31	–
	LC6	11.4	2	3.5–31	–
	LC7	5	2	8	3.3
	LC8	11.4	7.1	12.1	2.2
	LC9	18	7.1	12.1	2.2
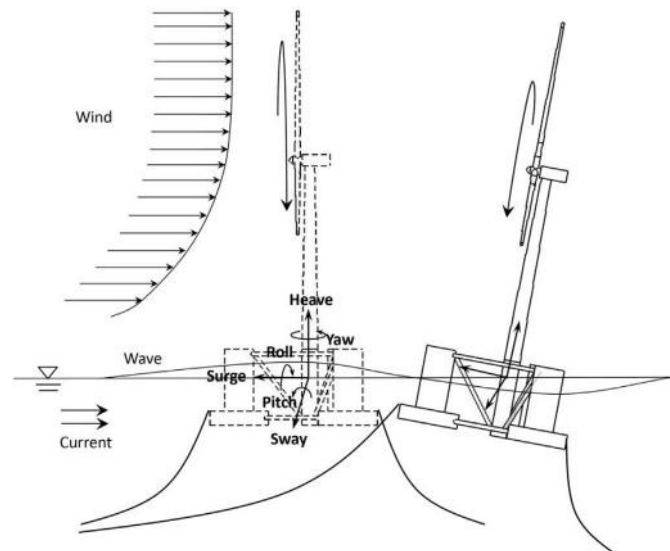
Fig. 10. 6-DOF motion of a semi-submersible FOWT.

fabricate the blades for the experiment. In addition, a geometrically similar blade has a mass of 137 g, which is slightly lighter. However, since the chord length of performance-matched blades is much larger than the design value (see Fig. 2), the mass of a performance-scaled blade is 832 g, which is overweight. Therefore, a correction method must be applied to account for the mass distribution in PMBS.

The mass properties for the wind turbine components, the supporting

platforms and the whole system, including the components of the design and the GMBS and PMBS models, are listed in Tables 2–4, respectively. The wind turbine of the PMBS model is inevitably overweight because of the high-mass performance-matched blades, in addition to the additional cables and sensors (see Table 2). The system mass distribution adjustment method is diagrammed in Fig. 4 (wherein, M_{PMBS}^{W} and M_{GMBS}^{W} denote the weight of the wind turbine between the two models, respectively. M_{PMBS}^{PT} and M_{GMBS}^{PT} denote the weight of the platform and the tower between the two models, respectively). The ballast weight of the PMBS model was decreased (see Table 3) to match the design value as much as possible. Nevertheless, the centre of mass (CM) of the entire PMBS system is still located at a higher point than the design value (see Table 4), but this is acceptable for model tests.

The sensors and their respective coordinated systems used for the experiments are shown in Fig. 5. The 1#load cell is installed at the joint between the tower and nacelle to measure the shear forces and bending moments at the tower-top interface. The 2#load cell is installed behind the rotor to measure the loads induced by the aerodynamic forces. An accelerometer located in the rear of the nacelle is used to measure the 3-DOF nacelle accelerations. The 6-DOF motion of the floating platform were measured by active optical markers installed near the base of the tower (see Fig. 3). In the 6-DOF reference coordinate system, the coordinate origin 'o' is located at the intersection point of the tower centreline and the still water surface, and the positive x coordinate-axis is directed opposite to the direction of propagation of the wind, wave and current during the tests.

2.3.2. Wind field test

The wind generation system, shown in Fig. 6, consists of nine independently controllable axial fans in a 3×3 frame configuration with a 3.75 m $\times$ 3.75 m wind field area, which satisfies the rotor coverage for extreme environmental conditions. To reduce turbulence, a honeycomb screen was used to cover the outlet of the wind generator system.

More details about the establishment of the wind field, the relationship between the measured wind speed and the thrust force, the quality of the model wind field and etc. can be found in the reference (Duan et al., 2016a). Some important measurements about the GMBS and PMBS model are listed in Table 5 for proofreading in the subsequent sections (wherein, 1P and 3P denote once and three times the rotor speed, respectively).

2.3.3. Model tower

The model tower (see Fig. 7) emulates the OC3-Hywind tower (Jonkman, 2010). In the test, an aluminum 6 061 alloy material was used to fabricate the model tower, due to its relatively low stiffness, light and
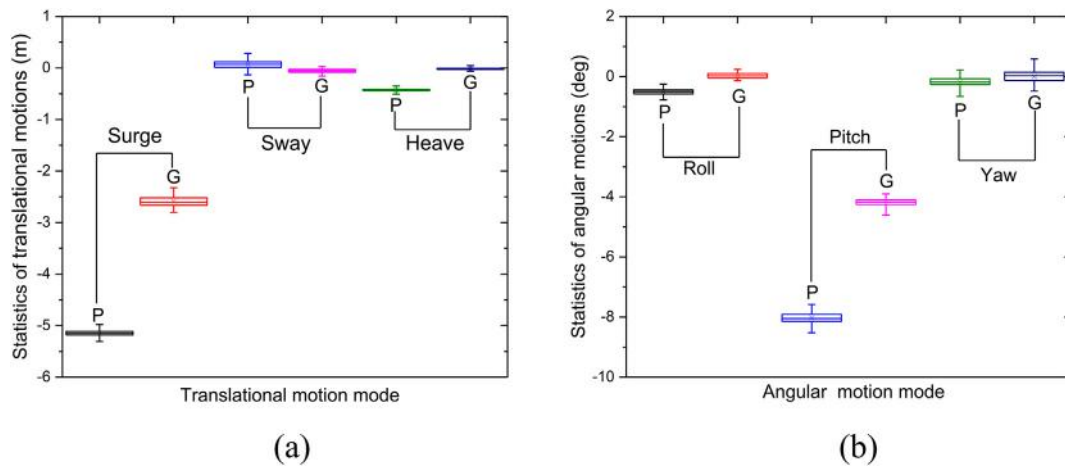
Fig. 11. Comparison of aero-induced motions in LC3.

Table 8
Statistics of F_{x2} and M_{x2} in LC3.

Statistics	F_{x2}/kN		M_{x2}/kN.m	
	PMBS	GMBS	PMBS	GMBS
Average	−1444.73	−1018.34	−6702.72	−1015.53
Range	403.92	311.06	2563.46	1441.04
Std.	70.31	50.17	503.30	381.22
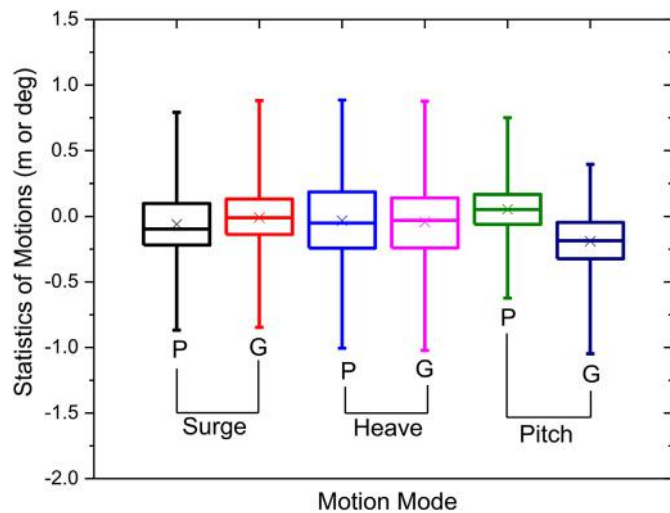
Fig. 12. Comparison of wave-induced motions in LC5.

Fig. 13. *RAOs of surge, pitch and heave motion of the PMBS model in LC5.*

2.3.4. Free-decay tests

The purpose of the free-decay tests is to identify natural frequencies and damping ratio of the 6-DOF motion. It should be noted that the rotor is parked and the wind generation system is shut down during the free-decay test. Test results are listed in Table 6 and comparisons of the PMBS and the GMBS models are shown in Fig. 9.

Fig. 9a indicates that there are some differences in the 6-DOF motion natural frequencies between the PMBS and the GMBS models, especially regarding the roll and pitch motion. This is because the overweight blades in the PMBS model produce a higher centre of gravity and less hydrostatic restoring during roll and pitch motion. Consequently, these changes yield smaller natural frequencies for roll and pitch motion in the PMBS model. On the other hand, the damping ratios of the PMBS model are slightly larger than that of the GMBS model during surge and sway motion (see Fig. 9b). This occurs because the aerodynamic damping of the PMBS model is greater than that of the GMBS model due to a larger area of the aerofoil section in the PMBS model. It should be noted that the rotor is parked during the free-decay tests; thus, the larger windward surface area of the PMBS model's blades corresponds to larger aerodynamic damping, but this circumstance is significantly different from revolving-blade conditions. Furthermore, aerodynamic damping is a

higher resistance to deterioration in wind/wave tests. In the hammer test, the model tower without the rotor and nacelle was rigidly connected to the land via a load cell that measured the bending moment caused by the tower vibration. Subsequently, to hit the model tower quickly with a hammer. The test result is shown in Fig. 8. The first peak at 2.63 rad/s is the first natural frequency of the model tower, and the second peak at 4.21 rad/s is the second natural frequency of the model tower. As the tower would be mounted on a floating platform in wind/wave tests, and the rotor-nacelle-assembly would be connected on the model tower top, the natural frequencies of the model tower maybe change a little bit in wind/wave tests. In addition, since the performance-matched blades are heavier than the geometrically matched blades, the natural frequencies of the model tower of the PMBS model could be different from those of the GMBS model, which will be discussed in section 3.3.1.
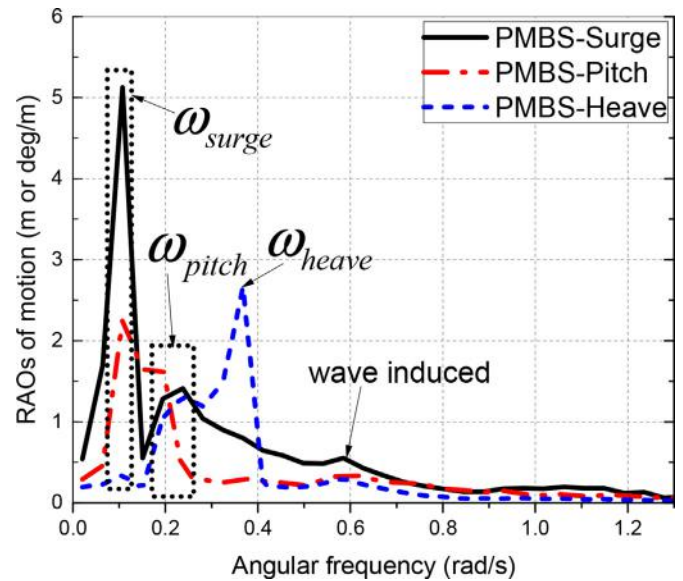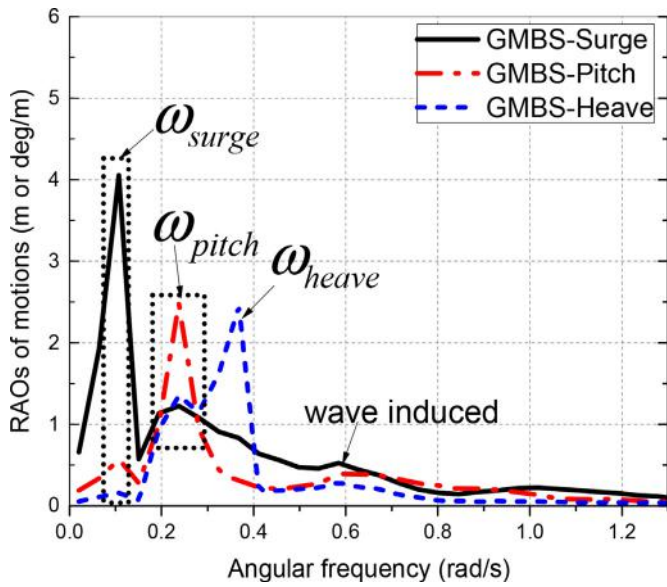
Fig. 14. *RAOs of surge, pitch and heave motion of the GMBS model in LC5.*

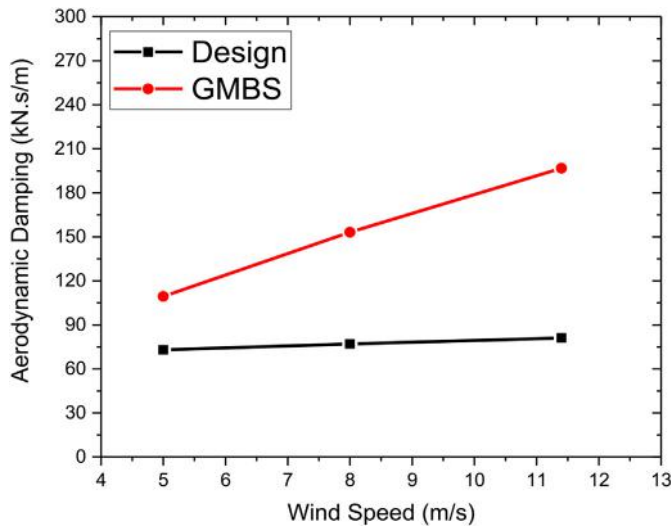**Fig. 16.** Comparison of surge motion in LC5 and LC6.

Fig. 15. Aerodynamic damping of the design and the GMBS model.

nonlinear and complicated phenomenon in FOWT revolving-blade conditions, which will be discussed in section 3.2.1.

2.4. Test matrix

The test matrix for wind-only cases (LC1-LC4), band-limited white-noise wave-only cases (LC5), and combined wind and irregular wave cases (LC6-LC9) are all listed in Table 7. In the table, *Hs* represents the significant wave height, *Tp* represents the spectral peak wave period, and *ɣ* represents the spectral peak parameter. It is worth noting that LC8 is a combination case of the rated wind speed (11.4 m/s) and a one-year return period of the Gulf of Maine wave (Koo et al., 2014).

3. Results and discussion

3.1. Comparison of 6-DOF motion

The 6-DOF motion (see Fig. 10) in the FOWT, including surge, sway, heave, roll, pitch and yaw motions, reflects the essential dynamical characteristics of the FOWT system. These motions exert an additional
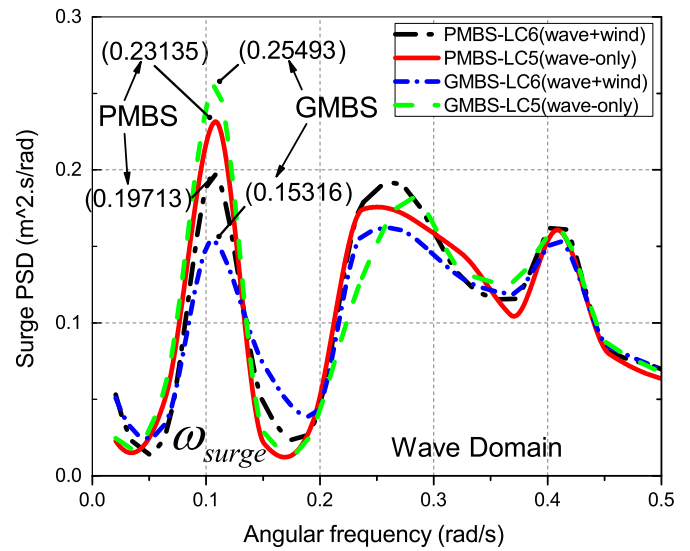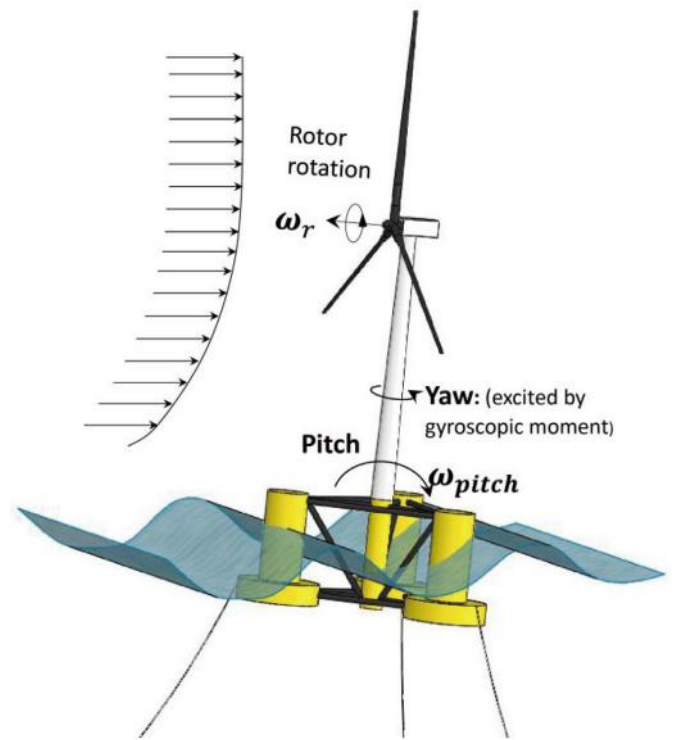

Fig. 17. Relationship between yaw, pitch and the revolving rotor.

influence on other FOWT components, such as the mooring system, the wind turbine, and the tower. Therefore, the 6-DOF motion and their coupled effects between two blades models are compared in this subsection to distinguish basic differences between the two blade concepts.

3.1.1. Aero-induced motions

It is well known that the PMBS model was proposed to improve the aerodynamic performance of FOWTs, but it is unfortunately characterized by overweight blades. Thus, there may be some differences in aero-induced motions between two model methods. The time-domain 6-DOF motion data in LC3 (wind-only case) between the two models is illustrated within boxplots in Fig. 11 (where the whiskers outside the box represent the minimum and maximum values; the lines in the box denote
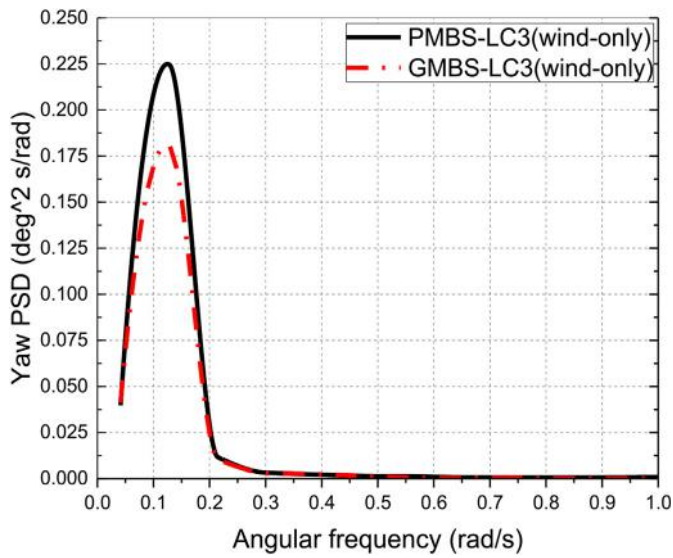
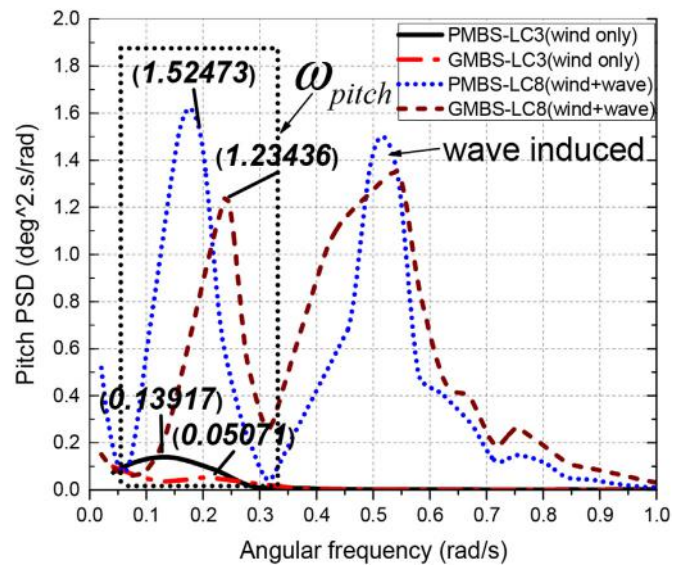Fig. 18. Comparison of yaw motion in LC3.

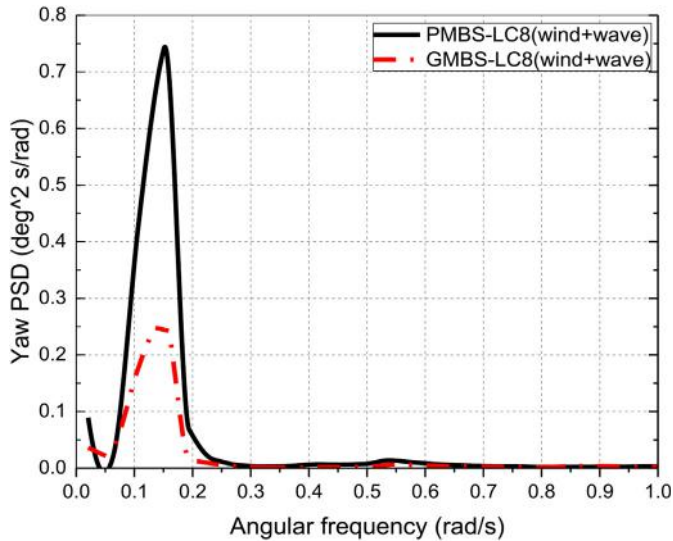Fig. 20. Comparisons of pitch motion in LC3 and LC8.

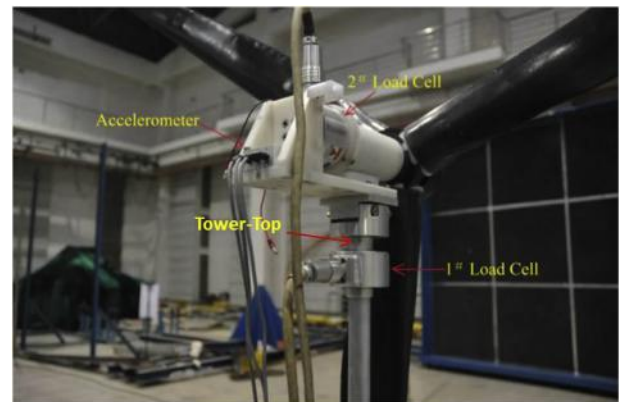Fig. 19. Comparison of yaw motion in LC8.

Fig. 21. Tower-top structure and sensors.

the upper quartile, the median and the lower quartile, respectively; the cross in the box indicates the average value; and 'P' denotes the PMBS model and 'G' denotes the GMBS model).

As shown in Fig. 11, aero-induced 6-DOF motion within the PMBS model are generally greater than those within the GMBS model, especially for surge and pitch motion. The difference in the surge motion between the models is due to the difference in the rotor thrust force between the models in LC3 conditions, as shown in Table 8 (wherein, F_{x2} and M_{x2} are the measured rotor thrust force and moment about the x-axis of the 2#load cell, defined in Fig. 5). The difference in the rotor thrust force between the models could be caused by the fact that the aerodynamic performance of the GMBS model was affected seriously by 6-DOF motion, and subsequently deteriorated during the test. The reason for the difference in the pitch motion and roll motion between the models is multifactorial. On the one hand, the PMBS model has a larger aerodynamic torque, which matches the design value better (see Table 8, M_{x2} and Fig. 1b, C_P). This larger aerodynamic torque in the PMBS model yields greater roll motion during the experiment. Similarly, the larger aerodynamic thrust force yields greater pitch motion during the test. On the other hand, the PMBS model is also influenced by the fact that the

overweight blades induce a higher centre of gravity and a smaller metacentric height for pitch and roll motion. Regarding the slight differences in the other motion modes, the reasoning is similar to that presented above; however, it should also be noted that the coupling motion and gyroscopic effects make the 6-DOF motion more complex and related to one another, the details of which will be detailed in the subsequent sections.

3.1.2. Wave-induced motions

Since the propagation direction of the wave is maintained as equal to zero during the tests (see Fig. 5), the dominant wave-induced motions are surge, pitch and heave motions. Statistics for the surge, pitch and heave motions in the white-noise wave case (LC5) are plotted in Fig. 12, which indicates that there is a good agreement between the models, with an exception for pitch motion. Since the wind generation system is turned off in LC5 (white-noise wave case), the slight difference in the pitch motion between the models is primarily due to the overweight blades in the PMBS model.

Surge, pitch and heave motions have notable coupling motion effects between one another, which is chiefly caused by the motion-induced imbalance in the mooring system, the motion-induced changes of the wet surface, etc. The results, which are presented in the form of *RAOs* (response amplitude operators of the system) of the surge, pitch and heave motions in LC5, are plotted in Fig. 13 and Fig. 14.
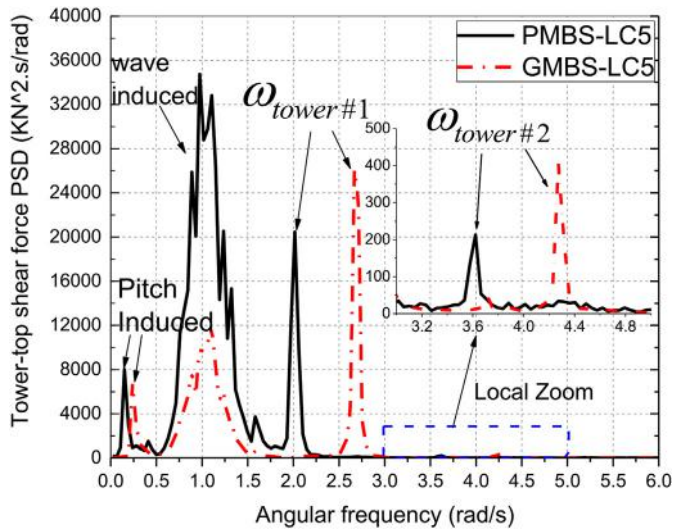
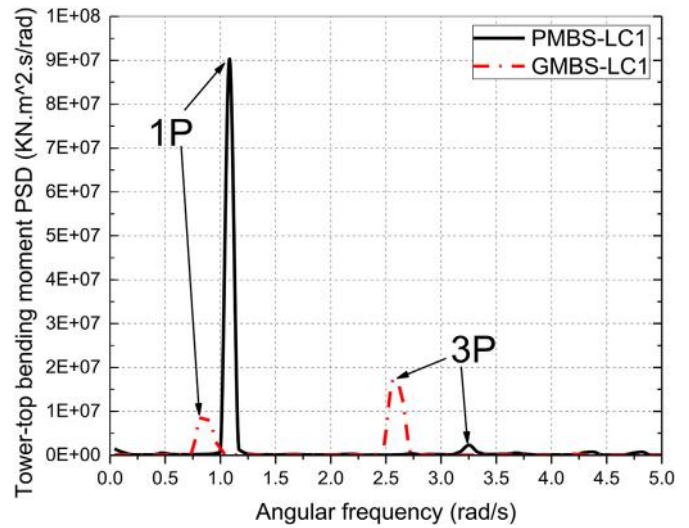**Fig. 22.** Comparison of the tower-top shear forces in LC5.

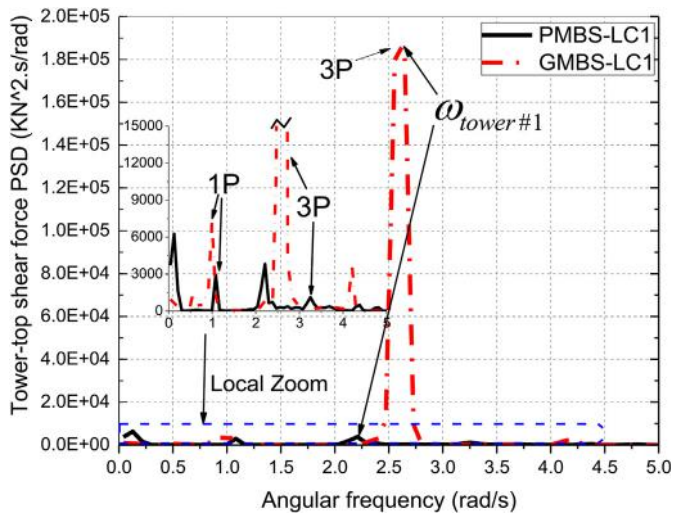**Fig. 25.** Comparison of the tower-top bending moment in LC1.

Fig. 23. Comparison of the tower-top shear forces in LC1.

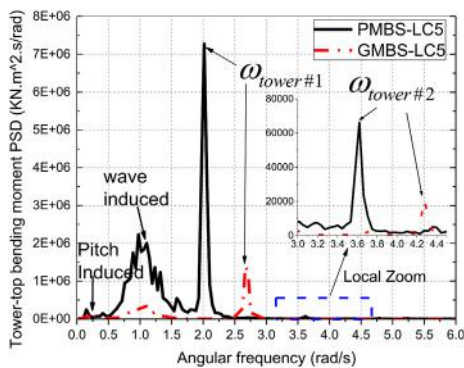**Fig. 26.** Construction of the mooring-lines system.

Fig. 24. Comparison of the tower-top bending moment in LC5.

As mentioned previously, the frequency range of the white-noise wave used in the experiment ranges from around 0.203 to 1.795 rad/s. Consequently, the significant resonant response in the surge motion was excited by second-order difference-frequency wave forces, and these
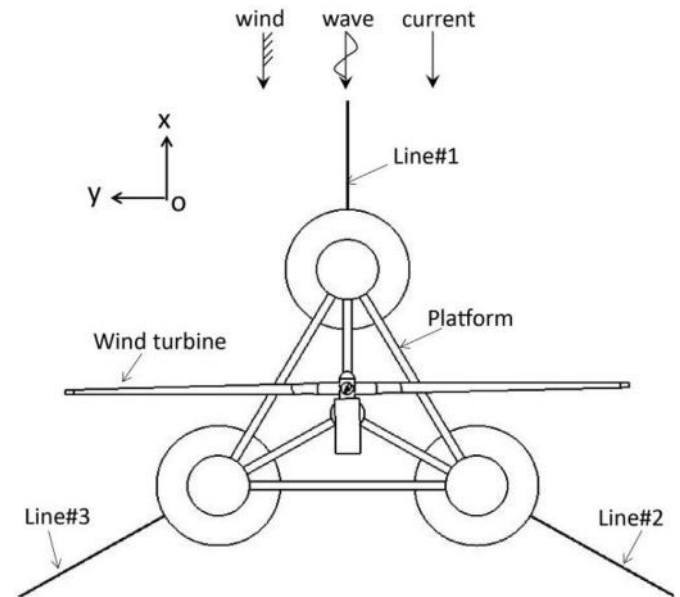
responses occurred in both models. Moreover, Figs. 13 and 14 show a strong coupling motion effect between the surge and pitch motion in both models. However, compared to the coupling motion effects in the GMBS model, this effects in the PMBS model are more distinct, which are primarily induced by the natural frequency discrepancy in pitch motion between the models. As shown in Table 6, the pitch natural frequency of the PMBS model is slightly smaller than that of the GMBS model and is closer to the surge natural frequency. When the pitch natural frequency and the surge natural frequency are relatively equivalent, the coupling motion effect between the surge and pitch motion will be more significant.

In general, either model method can reflect the essential 6-DOF motion characteristics, but there are some particular differences that should be noted with caution. Some of the differences principally originate from the discrepancy in the mass distribution, but others are sourced from the aerodynamic performance discrepancy between the models.
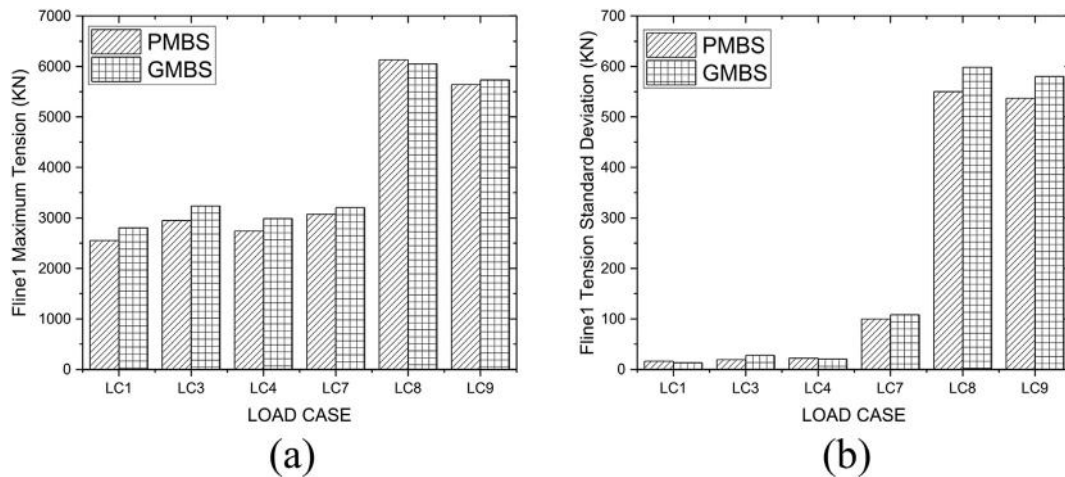
Fig. 27. Comparison of tension of the line#1: (a) maximum value. (b) standard deviation.
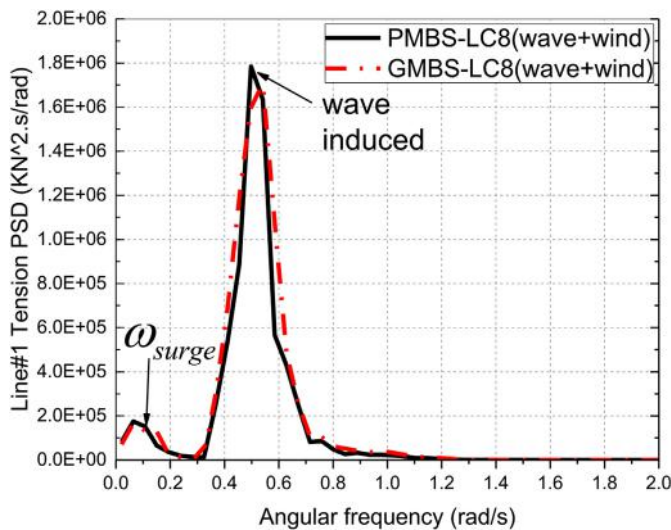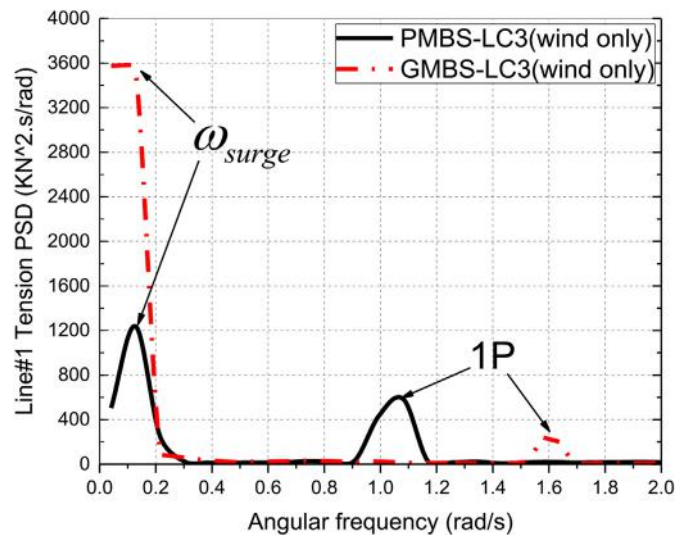

Fig. 28. Tension of the line#1 in LC8.

Fig. 29. Tension of the line#1 in LC3.

3.2. Comparison of aerodynamic characteristics

3.2.1. Aerodynamic damping

Aerodynamic damping usually plays an important role in reducing the wave-induced dynamic responses and fatigue damage in FOWTs (Karimirad and Moan, 2010; Cheng et al., 2016). Therefore, accurate simulation of aerodynamic damping in FOWT model experiments is also of great concern; thus, comparisons of the aerodynamic damping effects between the two models are discussed in this subsection.

Aerodynamic damping can be defined as the ratio of the thrust variation to the axial wind speed variation in a FOWT (Larsen and Hanson, 2007) as follows:

$$\delta_{aero} = \frac{\partial T}{\partial V} \tag{7}$$

where δ_{aero} is the so-called aerodynamic damping, ∂T is the variation of the aerodynamic thrust force, and ∂V is the variation of the axial wind speed.

The aerodynamic damping between the desired value (design) and the GMBS model below the rated wind speed (11.4 m/s) are compared in Fig. 15.

Fig. 15 illustrates that aerodynamic damping within the GMBS model

is much larger than within the desired value. As mentioned previously, the PMBS model's blades have more effective aerodynamic performances than those of the GMBS model under low-Reynolds-model conditions. Hence, it could be speculated that the PMBS may potentially have a higher fidelity in aerodynamic damping than that of the GMBS model. As a consequence of this possibility, a comparison of the aerodynamic damping effects between the PMBS and GMBS models was conducted, and the power spectral densities (PSD) of the surge motion between the two models in LC5 (wave-only case) and LC6 (combined wind and wave case) are compared in Fig. 16.

As is apparent from Fig. 16, the surge resonant responses appear to have been suppressed by aerodynamic damping effects in both models. Moreover, it is obvious that the PMBS model possesses a smaller aerodynamic damping effect. In other words, the PMBS model has a higher fidelity in aerodynamic damping than the GMBS model.

In summary, aerodynamic damping suppresses resonant responses significantly in both models. Compared to the larger aerodynamic damping observed in the GMBS model, the PMBS model has a higher fidelity. Furthermore, aerodynamic damping is a complicated and nonlinear aerodynamic effect, and could be affected by wind speed, aerofoil characteristics, 6-DOF motion, and other parameters. It is therefore suggested that aerodynamic damping be considered when designing model blades in the future. More investigations on the
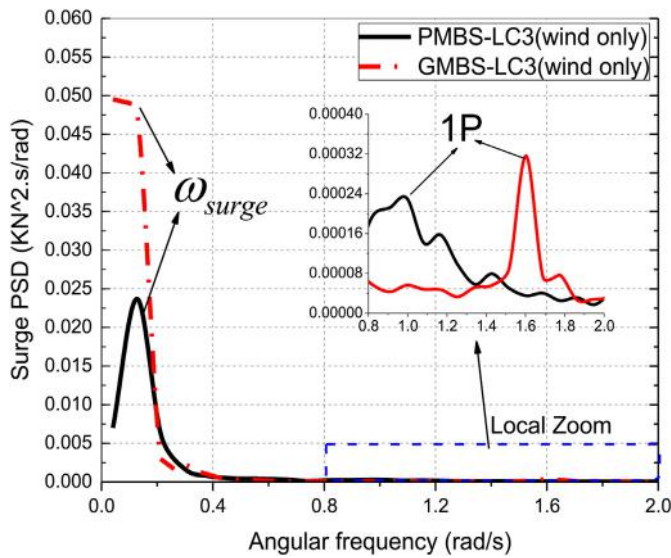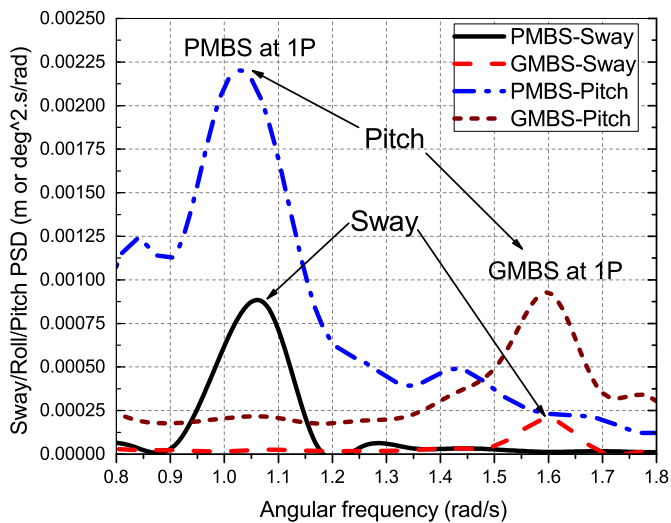
Fig. 30. Surge motion PSD in LC3.

Fig. 31. Comparison of sway and pitch motion *PSD* in LC3.

aerodynamic damping of a FOWTs can be found in the references (Chen et al., 2017).

3.2.2. Gyroscopic effects

When the rotor of an FOWT is rotating and is simultaneously combined with pitch motion, the yaw motion could be excited by the consequent so-called gyroscopic moments (Mostafa et al., 2012; Nematbakhsh et al., 2013) (see Fig. 17). Subsequently, yaw motion could yield asymmetric aerodynamic loads and thereafter induce an unfavourable impact on the sway motion, roll motion and even the power generation of the FOWT system during operation. Thus, comparisons of the gyroscopic effect between the two models are made and are discussed in this subsection.

Prior to further clarifying the effects of gyroscopic motion, relevant definitions must be made. Assume that the angle of the rotor induced by the motion of the floating supporting platform is slightly periodic motion, yielding:

$$\xi_i = \zeta_i^0 e^{-i\omega_i t} \quad (\text{i = pitch, roll or yaw}) \tag{8}$$

where i denotes the motion modes, ω_i is the angular velocity of the

floating platform with respect to the i th motion mode, ζ_i^0 is the amplitude of the rotational angle of the floating platform with respect to the i th motion mode.

According to Euler's equation, the gyroscopic moment, which makes the FOWT tend towards yaw motion, is given by (Mostafa et al., 2012; Nematbakhsh et al., 2013):

$$M_{yaw}^{\text{gyro}} = \left(I_{rx} - I_{ry}\right)i\omega_r\omega_{pitch}\xi_{pitch}^0 e^{-i\omega_{pitch}t} \tag{9}$$

where I_{rx} and I_{ry} are the moments of inertia of the rotor around the corresponding coordinate axes, ω_r is the rotational speed of the rotor, which is constant; ω_{pitch} is the angular frequency of the pitch motion. Note that the production of vibrational amplitude terms is neglected in this equation.

A comparison of the gyroscopic-moment-induced yaw motion between the two models in LC3 (wind-only case) and LC8 (combined wind and wave case) is illustrated in Figs. 18 and 19, respectively. As shown in Figs. 18 and 19, the most significant responses in the models both occur at the yaw motion natural frequency. On the other hand, it should be noted that gyroscopic-moment-induced yaw motion of the PMBS model is always greater than that of the GMBS model, and even the gap has been amplified from LC3 (wind-only case) to LC8 (combined wind and wave case). The reasons for the difference are multifactorial. It could be induced by the mass distribution discrepancy or the aerodynamic damping discrepancy between the models. As a consequence of the overweight blade in the PMBS model, the corresponding moment of inertia of the PMBS's rotor is larger, which yields a larger gyroscopic moment (see Eq. (9)). On the other hand, as mentioned previously, the aerodynamic damping of the PMBS is smaller, and the centre of gravity of the PMBS is higher, both of which additionally contribute to greater pitch motion in the PMBS model. These factors consequently contribute to larger yaw motion in rotor-revolving conditions according to Eq. (9).

To verify the inferences above, the pitch motions in the PMBS and GMBS models in LC3 (wind-only case) and LC8 (combined wind and wave case) are compared in Fig. 20. Fig. 20 indicates that the PSD of the pitch motion responses in the PMBS model are larger than that of the GMBS model, and the gap of the pitch motion is also amplified from LC3 (wind-only case) to LC8 (combined wind and wave case), which is in agreement with the observed variation in gyroscopic-moment-induced yaw motion illustrated in Figs. 18 and 19.

In summary, these two model methods both exhibit a gyroscopic effect despite some discrepancies in the response amplitudes. These discrepancies are potentially the consequence of aerodynamic damping discrepancies, or discrepancies in the blade weights between either model.

3.3. Comparison of the tower-top structures

The tower-top structure (see Fig. 21) is an important interface between the nacelle and the tower and is susceptible to simultaneous aerodynamic loads and 6-DOF motion (Xu and Ishihara, 2014). Thus, it is vital to accurately model the dynamical characteristics of the tower-top structure in the model tests. To compare the structural dynamical differences of the tower-top structure between the PMBS and GMBS models, the shear force and the bending moment in the tower-top structure are investigated (where the tower-top shear force in the x-axis is denoted by F_{x1} and the bending moment in the y-axis is denoted by M_{y1}). The relevant details regarding F_{x1} and M_{y1} can be found in Fig. 5.

3.3.1. Tower-top shear force

The shear force F_{x1} of the PMBS and the GMBS models in LC5 (white-noise wave case) is shown in Fig. 22, from which it is apparent that the F_{x1} dynamic response between the two models is similar and that the significant responses occur primarily within the wave-energy domain and at the tower eigenfrequencies. Nevertheless, there are also some significant differences that must be noted. Firstly, the tower

Table 9
Summary of dynamical characteristics between the two models.

Dynamic responses	Similarities	Differences	Differences Reasons
6-DOF motion	1 Surge resonant response is excited by second-order difference-frequency wave forces; 2 Coupling motion effects between surge and pitch motion are obvious.	1 Aero-induced 6-DOF motion of the PMBS model is greater than GMBS's generally; 2 More distinct coupling motion effects in the *PMBS* model.	1 Overweight blades of the PMBS model give rise to a higher centre of gravity. Moreover, aerodynamic performances of the GMBS model were affected seriously by the 6-DOF motion and deteriorated during the test; 2 Pitch natural frequency is closer to surge natural frequency in the PMBS model.
Aerodynamic damping	1 Aerodynamic damping suppress the surge resonant response significantly.	1 PMBS model possibly has a higher fidelity in aerodynamic damping than the GMBS model.	1 Wind speed in the *GMBS* model test was increased a lot to match the thrust forces, which aggravates aerodynamic damping in the GMBS model.
Gyroscopic effects	1 Both models can reflect the basic gyroscopic effect; 2 Gyroscopic effect is amplified in combined wind and wave cases.	1 The gyroscopic-moment induced yaw motion of the PMBS model is greater than that of the GMBS model; 2 Differences in yaw motion between models are amplified in combined wind and wave case.	1 Due to the discrepancy in the mass distributions and the aerodynamic damping between two models; 2 Discrepancy in pitch motion between two models is amplified in wind/wave cases, which gives rise to yaw motion differences.
Tower-top structure	1 Both models all can reflect basic dynamical properties of the tower-top structure.	1 The tower eigenfrequencies of the PMBS model are smaller than those of the GMBS model; 2 The tower-top shear and bending moment responses in the GMBS model are smaller than those of the PMBS model in wave-energy domain; 3 A huge difference at 3P frequency between two models	1 Tower eigenfrequencies are influenced by the different mass distributions between two models; 2 The PMBS model's blades are overweight, and gives rise to the wind turbine inertia loads; 3 3P frequency is close to the tower eigenfrequencies in the GMBS model.
Mooring-line system	1 Mooring lines are sensitive to wave loads rather than aerodynamic loads	1 There are small differences at the surge natural frequency and 1P aerodynamic frequency.	1 Due to the differences from the 6-DOF motion, which are caused by the mass distribution and aerodynamic differences between two models in fact.

eigenfrequencies in the GMBS model ($\omega_{1st}^{tower} = 2.667 rad/s$, $\omega_{2nd}^{tower} = 4.272 rad/s$) are larger than those of the PMBS model ($\omega_{1st}^{tower} = 2.016 rad/s$, $\omega_{2nd}^{tower} = 3.620 rad/s$) and are closer to the hammer test results ($\omega_{1st}^{tower} = 2.63 rad/s$, $\omega_{2nd}^{tower} = 4.21 rad/s$, see Fig. 8). This is because the tower eigenfrequencies are influenced by the different system mass distributions between either model, (e.g., it is known that the blades of the PMBS model weigh substantially more than those of the GMBS model). Secondly, the tower-top shear responses in the GMBS model are smaller than those of the PMBS model in the wave-energy domain. This can also be explained by the overweight blades of the PMBS model, which give rise to wind turbine inertia loads when the FOWT platform is subjected to wave loads and consequently oscillates.

The shear force F_{x1} of the PMBS and GMBS models in LC1 (wind-only case) is shown in Fig. 23. It can be observed that both models have significant responses at 1P and 3P periodic aerodynamic frequencies (wherein, 1P periodic loads are caused by some sort of the rotor imbalance; 3P periodic loads may originate from the interference of tower-shadow effects, non-uniform flow fields in space, and the incline of the floating supporting platform) and at the tower eigenfrequencies. Meanwhile, the substantial difference in the first tower eigenfrequency between the two models is due to the 3P frequency of the GMBS model, which is closer to the first tower eigenfrequency. Consequently, the tower resonates and yields significant shear responses in the GMBS model under these conditions.

3.3.2. Tower-top bending moment

The bending moment M_{y1} of the PMBS and GMBS models in LC5 (white-noise wave case) and LC1 (wind-only case) is plotted in Figs. 24 and 25, respectively. Fig. 24 illustrates that there are similar M_{y1} responses between the two models. Nevertheless, there are some differences in the wave-energy domain and at the first tower eigenfrequency. The likely reason for the discrepancy in the wave-energy domain is equivalent to that mentioned previously for the shear force. Meanwhile, the reason for the difference at the first tower eigenfrequency could be caused by the fact that the overweight blades of the PMBS model intensify the tower vibrations.

Fig. 25 demonstrates that the significant responses in both models primarily occur at 1P and 3P periodic aerodynamic frequencies, but the amplitude is notably different between either model. The difference in

M_{y1} at the 3P frequency is similar to that in the shear forces (see Figs. 23 and 25), and thus is also due to the tower resonant response in the GMBS model. However, the differences in M_{y1} at the 1P frequency are contrary to that in the shear forces (see Figs. 23 and 25). Taking into account that no other known characteristic frequency is close to the 1P frequency for the PMBS model, it is speculated that the tower-top bending moment response at the 1P frequency is also influenced by the overweight blades in the PMBS model.

In summary, both of the two models (i.e., PMBS and GMBS) can reflect basic tower-top structural dynamical properties, and they both show that the significant responses of the tower-top structure occur at the tower eigenfrequencies and the rotating-rotor-induced periodic aerodynamic frequencies. Nevertheless, there are still some discrepancies in the frequencies and response amplitudes between the models, which are primarily caused by the differences in the mass distribution between the models.

3.4. Comparison of the mooring system

The mooring system is important for a FOWT because it provides a fundamental position-anchoring function during horizontal motions (Hall and Goupee, 2015; Lin and Sayer, 2015). In this section, a series of comparisons of the mooring system between the two models are conducted to investigate the influences from the differences in mass distribution of the model blades and aerodynamic performances. The FOWT model mooring system consists of three catenary lines (shown in Fig. 26). Line#1 is aligned with the propagation direction of the wave, wind and current during the tests, and it is obvious that line#1 generally has a larger tension force than the other mooring lines. Therefore, line#1 is selected as the test object in this section. The maximum tension force and the standard deviation of the tension force for line#1 between the PMBS and GMBS models are compared in Fig. 27. Fig. 27 illustrates that there is a good agreement between the PMBS and GMBS models not only in terms of the maximum tension (see Fig. 27a) but also the standard deviation (see Fig. 27b).

The power spectral density (PSD) for the dynamic responses of line#1 between the models in LC3 (wind-only case) and LC8 (combined wind and wave case) are compared in Fig. 28 and Fig. 29, respectively. It demonstrates that the mooring line tension in LC8 (combined wind and wave case, see Fig. 28) is many times larger than that in LC3 (wind-only

case, see Fig. 29), and there is a better agreement between the two models in LC8. Therefore, these results indicate that the mooring line is more sensitive to the wave loads than the aerodynamic loads and that the dynamic responses of the mooring lines induced by the wave forces have a consistency between the two models.

Fig. 29 illustrates that there are some slight differences at the surge natural frequency and 1P aerodynamic periodic frequency. With the ambition of discovering the corresponding reason, the surge motion PSD between the two models in LC3 are compared in Fig. 30. It is readily apparent that the surge motion PSD in the GMBS model is larger than that in the PMBS model at the surge natural frequency, which agrees well with the mooring line response in Fig. 29. Nevertheless, it should be noted that the mooring line response at 1P frequency is different from the surge motion response at 1P frequency. Thus, it is speculated that the mooring line response at 1P frequency is also affected by other motions. To verify this conjecture, the sway and pitch motion between the two models are compared in Fig. 31. As is shown in Fig. 31, the sway and pitch motion at 1P frequencies in the PMBS model are all larger than those in the GMBS model. Thus, it can be concluded that the difference of the mooring line at the 1P frequency is caused by differences in the sway and pitch motions between the two models. The differences in these motions between either model are the result of the differences in mass distribution and aerodynamic performances, which have been analysed in section 3.1.

In general, the mooring line system is more sensitive to the wave loads than aerodynamic loads; thus, the differences in the mooring system dynamical behaviours between the two investigated models are quite small. In essence, these small differences are caused by the differences in both the mass distribution of the blades and the aerodynamic performances of the two models.

4. Conclusions

In this paper, a series comparisons of the OC4 semi-submersible offshore floating wind turbine models with the geometrically matched blades and the performance-matched blades were conducted, including 6-DOF motion, aerodynamic damping effects, gyroscopic effects, tower-top dynamic responses, and the mooring system's dynamical behaviors. The comparative results between two models are summarized in Table 9. In a word, both model methods can show the essential dynamical characteristics of the floating wind turbine, but some differences between two model methods should be noted. As shown in Table 9, compared to the GMBS model, the PMBS model has better aerodynamic performances, but has different mass distribution characteristics from the original design, which brings some changes for the PMBS model, including a higher centre of gravity, smaller natural frequencies of the pitch motion, the roll motion and the tower.

Acknowledgment

References

Coulling, A.J., Goupee, A.J., Robertson, A.N., Jonkman, J.M., Dagher, H.J., 2013. Validation of a FAST semi-type floating wind turbine numerical model with DeepCwind test data. J. Renew. Sustain. Energy 5 (2), 023116.

Chen, J., Duan, F., Hu, Z., 2017. Experimental investigation of aerodynamic damping effects on a semi-submersible floating offshore wind turbine. In: Proceedings of the 27th International Ocean and Polar Engineering Conference (San Francisco, USA).

Cheng, Z., Madsen, H.A., Gao, Z., Moan, T., 2016. Numerical study on aerodynamic damping of floating vertical axis wind turbines. J. Phys. Conf. 753 (10) (IOP Publishing).

Dunbar, A.J., Craven, B.A., Paterson, E.G., 2015. Development and validation of a tightly coupled CFD/6-DOF solver for simulating floating offshore wind turbine platforms. Ocean. Eng. 110, 98–105.

Duan, F., Hu, Z., Niedzwecki, J.M., 2016a. Model test investigation of a spar floating wind turbine. Mar. Struct. 49, 76–96.

Duan, F., Hu, Z., Liu, G., Wang, J., 2016b. Experimental comparisons of dynamic properties of floating wind turbine systems based on two different rotor concepts. Appl. Ocean Res. 58, 266–280.

Fowler, M.J., Kimball, R.W., Thomas, D.A., Goupee, A.J., 2013. Design and testing of scale model wind turbines for use in wind/wave basin model tests of floating offshore wind turbines. In: Proceedings of 32nd International Conference on Ocean, Offshore and Arctic Engineering (Nantes, France).

Gueydon, S., 2016. Aerodynamic damping on a semisubmersible floating foundation for wind turbines. Energy Procedia 94, 367–378.

Goupee, A.J., Fowler, M.J., Kimball, R.W., Helder, J., de Ridder, E.J., 2014. Additional wind/wave basin testing of the DeepCwind semi-submersible with a performance-matched wind turbine. In: Proceedings of 33rd International Conference on Ocean, Offshore and Arctic Engineering (California, USA).

Hall, M., Goupee, A., 2015. Validation of a lumped-mass mooring line model with DeepCwind semisubmersible model test data. Ocean. Eng. 104, 590–603.

Jonkman, J., 2010. Definition of the floating system for phase IV of OC3. Contract 1, 31.

Jonkman, J., Butterfield, S., Musial, W., Scott, G., 2009. Definition of a 5-MW Reference Wind Turbine for Offshore System Development. National Renewable Energy Laboratory, Golden, CO. Technical Report No. NREL/TP-500–38060.

Jeon, S.H., Cho, Y.U., Seo, M.W., Cho, J.R., Jeong, W.B., 2013. Dynamic response of floating substructure of spar-type offshore wind turbine with catenary mooring cables. Ocean. Eng. 72, 356–364.

Koo, B.J., Goupee, A.J., Kimball, R.W., Lambrakos, K.F., 2014. Model tests for a floating wind turbine on three different floaters. J. Offshore Mech. Arctic Eng. 136 (2), 020907.

Karimirad, M., Moan, T., 2010. Effect of aerodynamic and hydrodynamic damping on dynamic response of spar type floating wind turbine. In: European Wind Energy Conference (Poland, Warsaw).

Larsen, T.J., Hanson, T.D., 2007. A method to avoid negative damped low frequent tower vibrations for a floating, pitch controlled wind turbine. J. Phys. Conf. 75 (1) (IOP Publishing).

Lin, Z., Sayer, P., 2015. An enhanced stiffness model for elastic lines and its application to the analysis of a moored floating offshore wind turbine. Ocean. Eng. 109, 444–453.

Martin, H.R., 2011. Development of a Scale Model Wind Turbine for Testing of Offshore Floating Wind Turbine Systems (Doctoral dissertation, Maine Maritime Academy).

Ma, Y., Hu, Z., Xiao, L., 2015. Wind-wave induced dynamic response analysis for motions and mooring loads of a spar-type offshore floating wind turbine. J. Hydrodyn. Ser. B B 26 (6), 865–874.

Muliawan, M.J., Karimirad, M., Gao, Z., Moan, T., 2013. Extreme responses of a combined spar-type floating wind turbine and floating wave energy converter (STC) system with survival modes. Ocean. Eng. 65, 71–82.

Martin, H.R., Kimball, R.W., Viselli, A.M., Goupee, A.J., 2014. Methodology for wind/wave basin testing of floating offshore wind turbines. J. Offshore Mech. Arctic Eng. 136 (2), 020905.

Mostafa, N., Murai, M., Nishimura, R., Fujita, O., Nihei, Y., 2012. Study of motion of spar-type floating wind turbines in waves with effect of gyro moment at inclination. J. Nav. Architect. Mar. Eng. 9 (1), 67–79.

Nematbakhsh, A., Olinger, D.J., Tryggvason, G., 2013. A nonlinear computational model of floating wind turbines. J. Fluid Eng. 135 (12), 121103.

Robertson, A., Jonkman, J., Masciola, M., Song, H., Goupee, A., Coulling, A., Luan, C., 2012. Definition of the Semisubmersible Floating System for Phase II of OC4. Offshore Code Comparison Collaboration Continuation (OC4) for IEA Task, 30.

Robertson, A.N., Jonkman, J., et al., 2013. Summary of conclusions and recommendations drawn from the DeepCwind scaled floating offshore wind system test campaign. In: Proceedings of 32nd International Conference on Ocean, Offshore and Arctic Engineering (Nantes, France).

Wan, L., Gao, Z., Moan, T., 2014. Model test of the STC concept in survival modes. In: Proceedings of 33rd International Conference on Ocean, Offshore and Arctic Engineering, California, USA.

Wan, L., Gao, Z., Moan, T., 2015. Experimental and numerical study of hydrodynamic responses of a combined wind and wave energy converter concept in survival modes. Coast Eng. 104, 151–169.

Xu, N., Ishihara, T., 2014. Prediction of tower loading of floating offshore wind turbine systems in the extreme wind and wave conditions. Wind Eng. 38 (5), 463–476.